Scripta Materialia 250 (2024) 116207

Contents lists available at ScienceDirect

Scripta Materialia

journal homepage: www.journals.elsevier.com/scripta-materialia

Strain localization behavior in a polycrystalline magnesium alloy with de-twinning

Jongbin Go [a,b,**], Myeong-heom Park [a,*], Si Gao [a], Nobuhiro Tsuji [a,c]

[a] Department of Materials Science and Engineering, Kyoto University, Yoshida-honmachi, Sakyo-ku, Kyoto, 606-8501, Japan
[b] Department of Structure and Nano-/Micromechanics of Materials, Max-Planck-Institute for Sustainable Materials, Max-Planck-Straße 1, 40237 Düsseldorf, Germany
[c] Elements Strategy Initiative for Structural Materials (ESISM), Kyoto University, Yoshida Honmachi, Sakyo-ku, Kyoto 606-8501, Japan

ARTICLE INFO

Keywords:
Magnesium
Inhomogeneous deformation
De-twinning
Digital image correlation (DIC)

ABSTRACT

In this study, we present a distinctive phenomenon of strain localization observed in pre-strained AZ31 alloy during tensile deformation. The strain localization behavior involves the repetitive formation, propagation, and subsequent annihilation of localized deformation bands within the gage section of the specimen. Although this strain localization behavior bears resemblance to the Portevin–Le Chatelier (PLC) effect commonly observed in steels and Al-Mg alloys, it is driven by a fundamentally different mechanism. Through detailed microstructural analysis, we reveal that this unique strain localization is closely associated with the process of de-twinning. Our findings contribute to a deeper understanding of the deformation behavior in magnesium alloys and offer new insights for the strain localization in metals.

In recent years, reducing the weight of various products has become an important issue for conserving natural resources, saving energy, and reducing carbon dioxide emissions from transportation [1–3]. Magnesium is a candidate material for manufacturing lightweight products, owing to its low density of 1.738 g/cm^3, which is two-thirds the density of aluminum alloys and one-fifth that of steel. However, the poor room-temperature formability of magnesium alloys hinders their practical use [4]. The limited formability results from the magnesium alloys having a hexagonal close-packed (HCP) crystal structure with only two independent preferential slip systems (basal $\langle a \rangle$ slip), which cannot introduce displacement in the c-axis direction and satisfy the von-Mises criterion that requires five independent slip systems for arbitrary deformation [5]. Thus, additional deformation modes containing c-axis components are required for successful plastic deformation of magnesium alloys.

It is known that {10–12} twinning or de-twinning is an important deformation mode that can cause displacement in the *c*-axis direction of an HCP structure. This type of twinning tends to occur when the (0001) basal plane of the HCP lattice is parallel to the compression axis or perpendicular to the tensile axis; de-twinning is the reverse process in which loading in the opposite direction results in the twins disappearing and only the parent grains remaining [6,7]. The orientation dependence of twinning/de-twinning can be understood in terms of the Schmid factor for a {10–12} twin [8]. The occurrence of {10–12} twinning or de-twinning not only changes the orientation of the crystallographic lattice relative to the parent grain by approximately 86.3° [9], but also reduces the internal stress of the parent grain and twin resulting in significant stress relaxation [10,11].

In AZ31 commercial Mg alloys, macroscopic heterogeneous deformation bands have been observed in the deformation mode in which a {10–12} twin or a de-twin occurs [12,13]. Barnett et al. [12] observed Lüders bands during compression deformation of AZ31 Mg alloy, in which a {10–12} twin was the predominant deformation mode; the bands propagated progressively over the sample. Anten et al. [13] reported the formation and discontinuous propagation of macroscopic deformation bands, which they called twin bands, when {10–12} twinning or de-twinning behavior occurred repeatedly in AZ31 Mg alloy during cyclic tension-compression loading. While the above studies confirmed the existence of macroscopic heterogeneous bands, detailed analyses such as an analysis of dynamic band propagation/evolution during deformation have not been conducted.

Recently, the digital image correlation (DIC) technique, which can provide information on the local strain distribution, has been used for the characterization of heterogeneous deformation bands such as Lüders

** Corresponding author at: Department of Materials Science and Engineering, Kyoto University, Yoshida-honmachi, Sakyo-ku, Kyoto, 606-8501, Japan.
* Corresponding author.
E-mail addresses: j.go@mpie.de (J. Go), park.myeongheom.8r@kyoto-u.ac.jp (M.-h. Park).

https://doi.org/10.1016/j.scriptamat.2024.116207
Received 5 May 2024; Received in revised form 21 May 2024; Accepted 26 May 2024
Available online 2 June 2024

bands and Portevin–Le Chatelier (PLC) bands observed in some specific metallic materials (e.g., high-Mn steel [14–16], Al-Mg alloy [17,18], and NiTi shape memory alloys [19,20]). The behavior of strain-localized bands during deformation can be effectively characterized through DIC strain analysis in association with the occurrence of twinning/de-twinning. In the present study, we observed a unique deformation behavior in AZ31 Mg alloy during uniaxial tensile deformation, and we attempted to determine the underlying mechanism by examining the relationship between de-twinning and macroscopic heterogeneous deformation. AZ31 Mg alloy with about 50% volume fraction of twins was prepared by pre-compression, and it was subjected to tensile testing along different tensile axes to control the amount of de-twinning (i.e., twin → matrix). The local deformation behavior was quantitatively characterized by performing DIC analysis.

Commercial hot-rolled AZ31 Mg alloy (Mg-3.1%Al-1.1%Zn-0.3% Mn, wt%) was used in this study. The received plate was cut into a rectangular parallelepiped bulk with dimensions of 30 mm (length) × 60 mm (width) × 20 mm (thickness), homogenized at 400 °C for 2 h in an electrical box furnace, and air-cooled (Fig. 1(a)). The homogenized specimen was compressed by 4.5% in the width direction using a universal tensile/compression testing machine (Shimadzu, AG-100 kN Xplus) to form {10–12} twins in the matrix (Fig. 1(b)).

Two-millimeter-thick sheets were cut from the 4.5% pre-strained bulk sample, and tensile specimens with a 10 mm gage length and a 3 mm gage width were machined from the sheets. Tensile specimens having inclination angles of 0°, 45°, and 90° with respect to the compression angle were prepared (Fig. 1(c)), and they are hereafter referred to as 0°, 45°, and 90° specimens. The tensile specimens were polished to 1.5 mm thickness, and a speckle pattern was introduced on the polished surface with black and white inks for DIC strain analysis. The tensile properties were determined through tensile tests (Shimadzu, AG-100 kN Xplus) at room temperature and with an initial strain rate of $1.0 \times 10^{-3}\ s^{-1}$. The tensile specimen's image was captured by a CMOS camera with a constant capture speed of 5 frames per second during deformation. The recorded images with a resolution of 2432 pixels × 2054 pixels were used for the DIC strain analysis that was performed with a dedicated DIC software (VIC-2D, Correlated Solutions Inc.); a step size of 9 pixels and a subset size of 35 pixels were used in the analysis.

Microstructures were observed using a field-emission scanning electron microscope (JEOL, JSM-7100F) equipped with an electron backscatter diffraction (EBSD) detector, with a step size of 0.9 μm. Before the observation, a grinding process involving 120–4000 grit abrasive papers was performed, and the surface was polished with 1 μm diamond suspension and 0.02 μm colloidal silica. Information on crystallographic orientation was obtained using the software TSL OIM Analysis 7 × 64. The average grain size was determined using the line intercept method on the EBSD inverse pole figure (IPF) map.

Figs. 1(d) and (e) show EBSD IPF maps along with (0002) and (10–10) pole figures of the homogenized and pre-strained specimens, respectively. The homogenized specimen in Fig. 1(d) shows an equiaxed grain structure with an average grain size of 25.3 μm with a strong basal texture. On the other hand, in Fig 1(e), the pre-strained specimen has a much smaller average grain size of 6.3 μm owing to the formation of abundant {10–12} twins. The basal planes of the {10–12} twins were oriented in the transverse direction (TD) relative to the rolled plate, and their prism planes were broadly distributed in the rolling direction (RD). The grain boundary map of the pre-strained specimen is shown in Fig. 1(f), and the area fraction of the {10–12} twins was 49.0%.

Fig. 2 shows nominal stress-strain curves for the 0°, 45°, and 90° specimens. The tensile properties of the specimens are presented in Table 1. The 0° specimen showed a convex downward and low-slope plateau region after yielding. The plateau region progressed up to about 4% of the nominal strain, and then the stress increased rapidly with an increase in the strain. It is well known that {10–12} twinning or de-twinning is the primary deformation mode in the plateau region [6,21]. As the tensile angle increased from 0° to 90°, the tensile properties

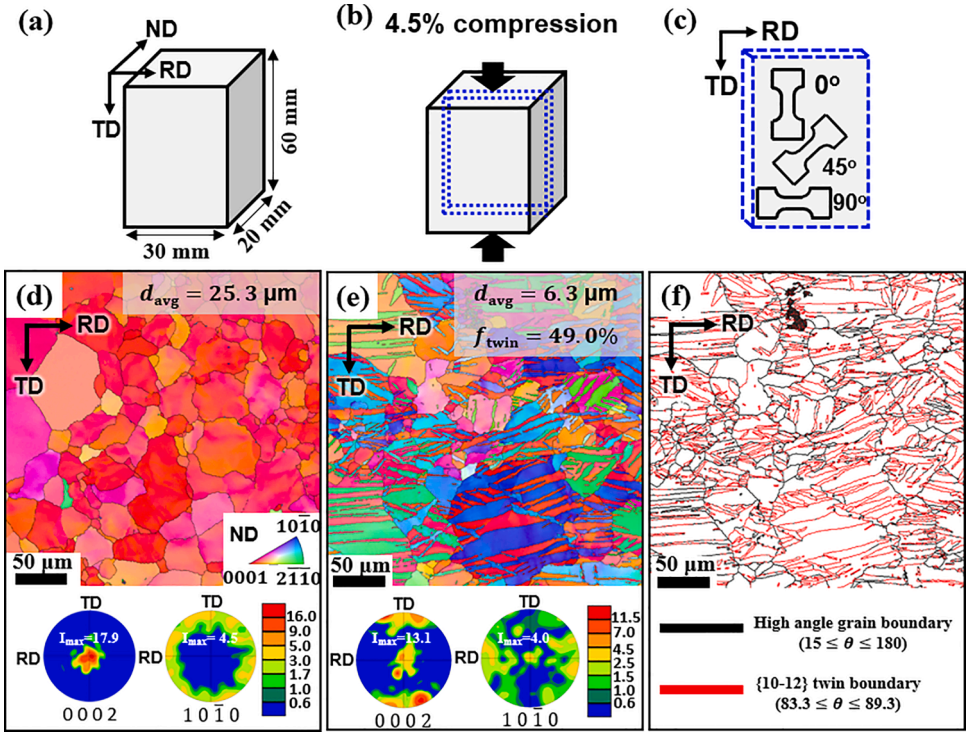

Fig. 1. Schematic illustration of (a) the homogenized sample treated at 400 °C for 2 h, (b) the 4.5% pre-strained sample in the TD direction after homogenization, where the blue dashed lines represent the sheet with a thickness of 2 mm to cut tensile specimens, and (c) tensile specimens sectioned as 0°, 45°, and 90° from TD. EBSD Inverse pole figure maps, (0002) and (10–10) pole figures of (d) as-homogenized and (e) pre-strained AZ31 Mg alloy. (f) High angle boundaries (HAGBs) and {10–12} twin boundaries (TBs) of the pre-strained AZ31 Mg alloy are indicated as black and red line lines, respectively. The d_{avg} and f_{twin} indicate the average grain size and the area fraction of {10–12} twin, respectively.

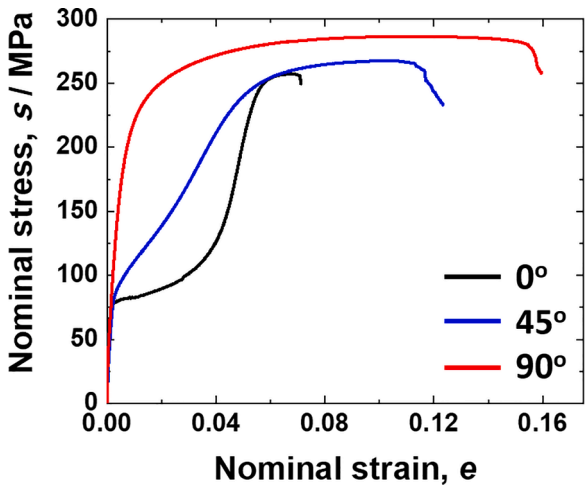

Fig. 2. Tensile nominal stress-strain curve of the 0°, 45°, and 90° specimens.

Table 1
Tensile properties of 0°, 45°, and 90° specimens.

Alloy	Tension		
	YS (MPa)	UTS (MPa)	EL (%)
0° specimen	68	270	9.2
45° specimen	94	267	11.3
90° specimen	207	286	15.9

TYS, UTS, and EL denote yield strength, ultimate tensile strength, and total tensile elongation, respectively.

changed significantly. The nominal stress of the 45° specimen tended to increase almost linearly after yielding. By contrast, the 90° specimen exhibited a stress-strain curve whose shape was similar to that observed for polycrystal metallic materials exhibiting smooth strain hardening after yielding. Such differences in the deformation behavior that depend on the direction of the tensile axis of the tensile specimens originate from changes in the de-twinning behavior [21,22].

Fig. 3 shows the DIC strain rate maps of the three specimens at several tensile strains in a very early stage of tensile deformation ($e < 0.01$). An interesting feature is that the 0° and 45° specimens exhibited inhomogeneous distribution of the strain rate in their gage part, which indicates that plastic strain localization occurred during the tensile deformation of the specimens even at such an early stage of deformation. The magnitude of strain localization was different in the three types of specimens. The 0° specimen showed intense strain localization, whereas the 90° specimen showed very weak strain localization. A strain-localized band was formed in the lower part of the 0° specimen's gage at a nominal strain of 0.00751 (Fig. 3(a)), and the local strain rate was 0.0047 s^{-1}, which was 4.7 times the global strain rate (0.001 s^{-1}). The band propagated upward while maintaining an almost constant local strain rate of 0.0043 s^{-1}, as shown in Fig. 3(b). Interestingly, with further propagation of the band, two new bands with lower local strain rates formed below it (Fig. 3(c)). Notably, the width of the upper band decreased with the formation of these two new bands, compensating for the decrease in its width. The three bands then propagated upward, redistributing the local strain rate (Fig. 3(d)) and eventually merged to form a single band with a high local strain rate (0.0045 s^{-1}) in the shoulder part (Fig. 3(e)). Subsequently, a new band was formed below the merged band (Fig. 3(f)), and the former band was annihilated as the strain rate of the newly formed band increased. The formation and propagation of multiple strain-localized bands with a high strain rate was also observed in the 45° specimen, but with a much lower strain rate in each band, as shown in Figs. 3(h)–(n). By contrast, no such strain localization behavior was observed in the 90° specimen (Fig. 3(o)-(t)).

To clarify the strain localization behavior, we determined the change in the strain rate distribution along the specimen's gage part as a function of the deformation time, and the obtained results are shown in Fig. 4. As shown in Fig. 4(a), the 0° specimen started to exhibit noticeable strain localization from 14 s, which is the instant when yielding occurred. The strain localization appeared at the bottom of the gage

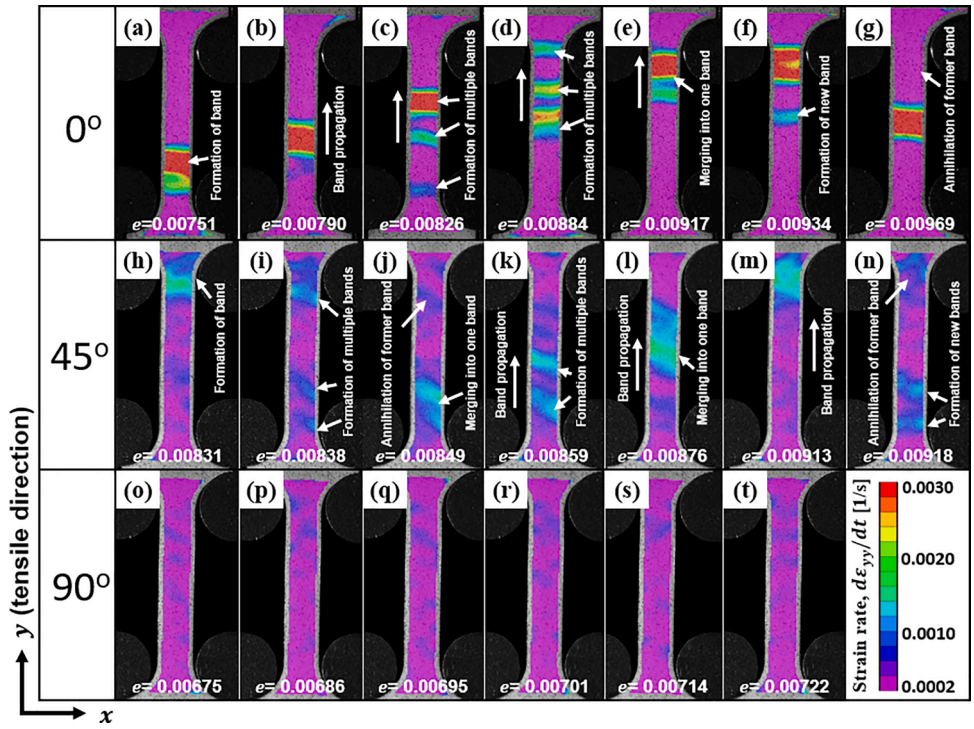

Fig. 3. DIC strain rate maps showing loading direction dependence on strain localization behavior during tensile deformation with increasing nominal strain after 0.2% offset yielding of (a-g) 0°, (h-n) 45°, and (o-t) 90° specimens, respectively. Nominal strain of each figure is indicated at the bottom.

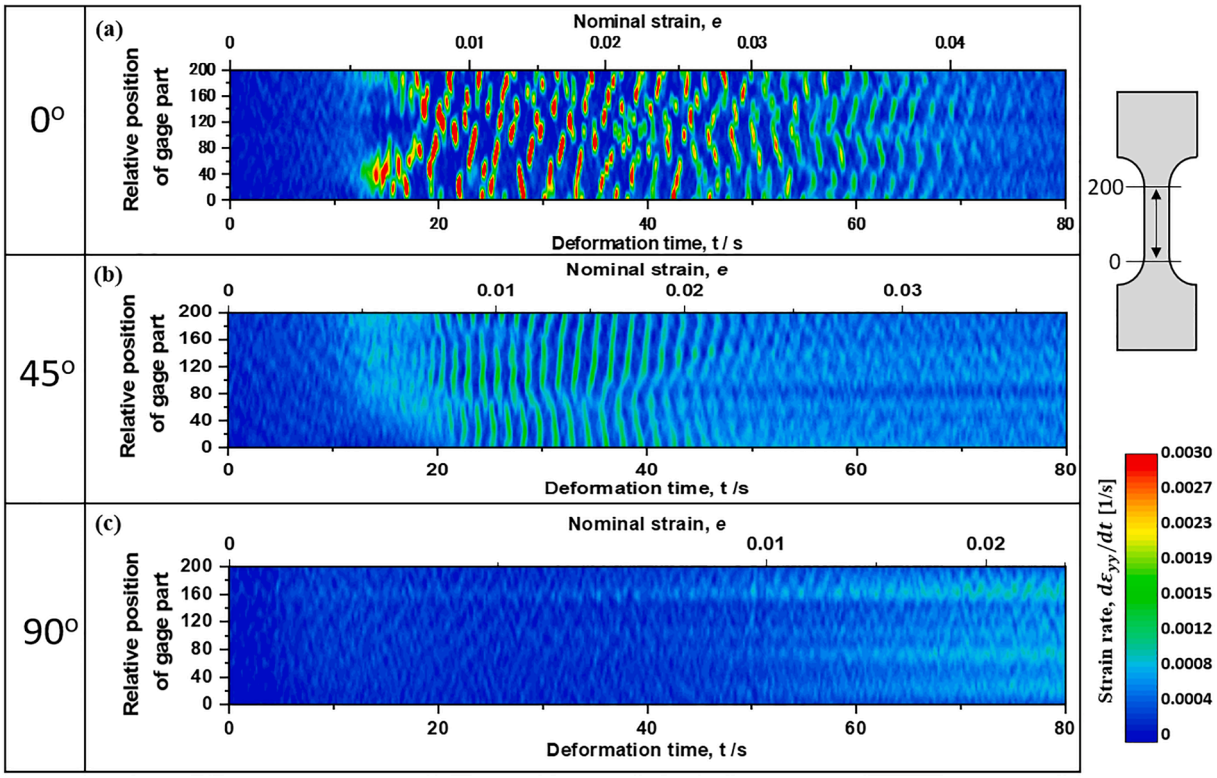

Fig. 4. Contour maps showing how strain rate in gage part changes with deformation time in the (a) 0°, (b) 45°, and (c) 90° specimens, respectively. Color gradients indicate the value of the strain rate. Here, the relative position of the gage part was obtained by dividing the gage part into 200 regions at each moment. The number from 0 to 200 represents the relative position of the gage part of the tensile specimen.

part. A strain-localized region with a high strain rate value of 0.003 s^{-1} was repeatedly formed, it propagated, and it was eventually annihilated in the gage part (refer to supplementary video 1). The strain rate of the strain-localized bands gradually decreased with increasing time. Furthermore, the inhomogeneous deformation caused by the strain-localized band occurred from 14 s (i.e., the instant the 0° specimen yielded) to 70 s, which corresponds to the yield plateau of the stress-strain curve of the 0° specimen. After 70 s, the specimen started to deform homogeneously. The repeated formation, propagation, and annihilation of strain-localized bands were also observed in the 45° specimen (Fig. 4(b)), but the strain rate of the strain-localized band was somewhat low, as already explained in the context of Fig. 3 (refer to supplementary video 2). Such strain-localized bands repeatedly occurred from the instant the specimen yielded up to 50 s. However, the

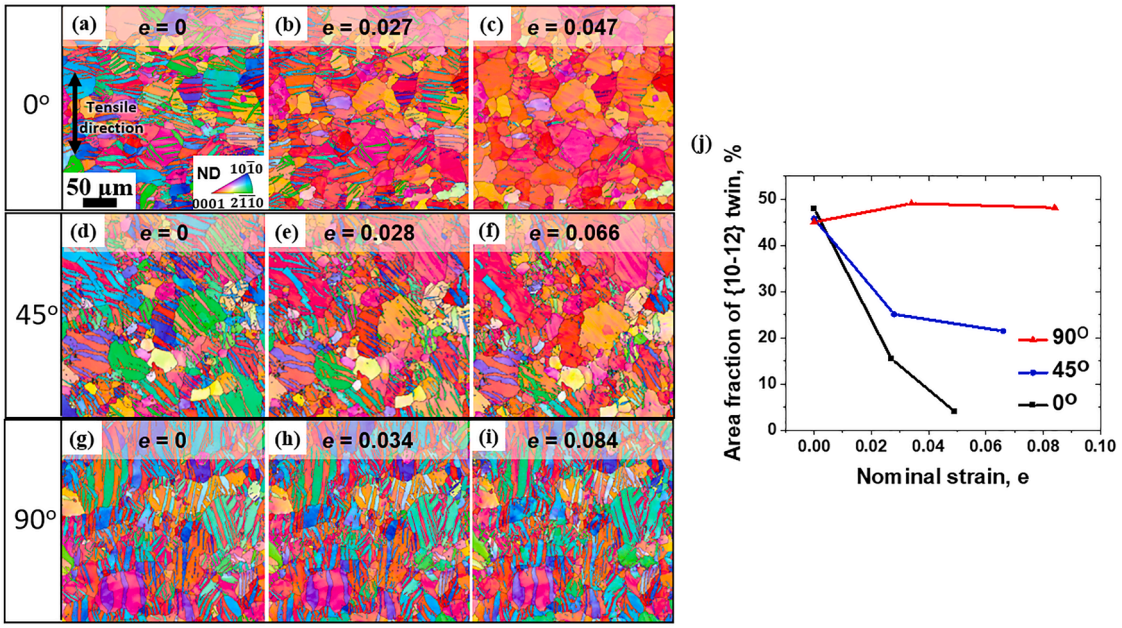

Fig. 5. Inverse pole figure maps showing differences in de-twinning behavior of (a-c) 0°, (d-f) 45°, and (g-i) 90° specimens with increasing nominal strain: (a) 0, (b) 0.027, (c) 0.047, (d) 0, (e) 0.028, (f) 0.066, (g) 0, (h) 0.034, and (i) 0.084. Graph (j) shows the area fraction of {10–12} twin as a function of nominal strain.

90° specimen did not show any intense inhomogeneous deformation resulting from strain-localized bands in Fig. 4(c) (refer to supplementary video 3).

To investigate the mechanism underlying the unique strain localization behavior of the specimens, we performed EBSD measurements at different tensile strains in the same observation areas on the 0°, 45°, and 90° specimens, and the results are shown in Fig. 5. In Fig. 5(a)–(c), the 0° specimen shows notable de-twinning as the tensile strain increases from 0 to 0.049. It is well known that de-twinning is the primary deformation mode when the loading direction is opposite to the compression direction in pre-strained AZ31 alloy, especially in the plateau region of the stress-strain curve [21,22]. For the 45° specimen, as shown in Figs. 5(d)–(f), de-twinning occurred during tensile deformation, but it was much less intense compared with the 0° specimen. In contrast to the 0° and 45° specimens, the 90° specimen showed a very small amount of de-twinning up to a nominal strain of 0.084, as shown in Fig. 5(g)–(i). The area fraction of the {10–12} twins during tensile deformation is shown in Fig. 5(j). The area fraction for the 0° specimen decreased significantly from 48% before tensile deformation to 15.5% at $e = 0.027$ and then continued to decrease to 4.1% at $e = 0.047$. In comparison, the 45° specimen showed a slower decrease in the twin fraction with increasing nominal strain. The area fraction of the {10–12} twins remained almost unchanged in the 90° specimen. Such significantly different de-twinning behavior can be explained by considering the change in the Schmid factor for the de-twinning of {10–12} twins. It should be noted that the Schmid factor for de-twinning increases when the angle between the *c*-axis and the loading direction decreases from 90° to 0° [8]. Therefore, the de-twinning of the {10–12} twin occurs more easily as the loading angle of the tensile specimen decreases from 90° to 0°

It should be noted that strain-localized bands were formed only in the 0° and 45° specimens that showed de-twinning behavior. The strain-localized bands were intensively formed in the plateau region of the 0° specimen (Fig. 4(a)). It is well known that twinning or de-twinning mainly occurs in the yield plateau [6,21,22]. The 90° specimen neither showed de-twinning behavior nor the formation of such a strain-localized band during deformation. Such correlation of the extent of de-twinning behavior with the intensity of the strain localization behavior strongly suggests that the unique strain localization behavior in the AZ31 alloy was associated with de-twinning. These results suggest that de-twinning may promote the formation of strain-localized bands. Another point to emphasize is that the strain-localized band frequently disappears during propagation, and the directional regularity sometimes collapses, resulting in chaotic propagation. Additionally, there was no noticeable serrated flow in the stress-strain curve of the AZ31 Mg alloy (Fig. 2). The absence of serrated flow in the AZ31 Mg alloy with de-twinning requires further investigation.

It is known that twinning/de-twinning occurs when (i) the dislocation slip is difficult to activate and (ii) the *c*-axis of the HCP structure is parallel to the tensile direction in the Mg/Mg alloy system. The 0° specimen in the present study satisfied both conditions (i) and (ii). When deformation by dislocation slip was difficult, de-twinning eventually occurred in the 0° specimen. However, this appears to have been a local event initiated from a region where de-twinning could easily occur. Once de-twinning occurs in some regions, it may promote de-twinning in neighboring grains in a chain reaction, resulting in the propagation of a strain-localized band. Considering that the twinning/de-twinning phenomenon is a type of stress relaxation process [10,11], we can infer that stress relaxation can be the reason for band propagation to the neighboring grains to activate de-twinning. The underlying mechanism for the local occurrence of twinning/de-twinning is still unclear, but it can be understood through in situ characterization of microstructure evolution, which will be done in our next research work. Nevertheless, the present study clearly shows that de-twinning significantly affects macroscopic deformation behavior by inducing macroscopic strain-localized bands. This suggests that the formation mechanism of the strain-localized bands observed in this study is entirely different from that of the PLC bands caused by dynamic strain aging (DSA), which results from interactions between dislocations and solute atoms [23–26].

In this study, we report the observation strain-localized bands similar to the Portevin–Le Chatelier (PLC) band, in pre-strained AZ31 Mg alloy for the first time. In particular, the formation, propagation, and annihilation of the bands were repeatedly observed in the plateau region of the stress-strain curve for the 0° specimen that exhibited significant de-twinning behavior. The local strain rate in these bands increased as the de-twinning behavior was intensively activated. These results imply that the strain localization behavior is likely to have resulted from de-twinning, not because of DSA. Further research is required to ascertain whether de-twinning promotes such strain-localized bands during tensile deformation.

CRediT authorship contribution statement

Jongbin Go: Writing – review & editing, Writing – original draft, Visualization, Validation, Project administration, Methodology, Investigation, Funding acquisition, Formal analysis, Data curation, Conceptualization. **Myeong-heom Park:** Writing – review & editing, Writing – original draft, Validation, Supervision, Project administration, Funding acquisition, Conceptualization. **Si Gao:** Writing – review & editing, Writing – original draft, Validation, Supervision, Methodology, Investigation. **Nobuhiro Tsuji:** Visualization, Validation, Supervision, Project administration, Conceptualization.

Declaration of competing interest

The authors declare that they have no known competing financial interests or personal relationships that could have appeared to influence the work reported in this paper.

Acknowledgments

This study was financially supported by JST CREST (JPMJCR1994), Elements Strategy Initiative for Structural Materials, and JSPS KAKENHI Grant Numbers JP20H00306, JP20K14608, and JP22J14626, all through the Ministry of Education, Culture, Sports, Science and Technology (MEXT), Japan.

Supplementary materials

Supplementary material associated with this article can be found, in the online version, at doi:10.1016/j.scriptamat.2024.116207.

References

[1] F. Cuenot, CO_2 emissions from new cars and vehicle weight in Europe; How the EU regulation could have been avoided and how to reach it? Energ. Policy 37 (2009) 3832–3842.
[2] W.J. Joost, Reducing vehicle weight and improving U.S. energy efficiency using integrated computational materials engineering, JOM 64 (2012) 1032–1038.
[3] R. Huang, M. Riddle, D. Graziano, J. Warren, S. Das, S. Nimbalkar, J. Cresko, E. Masanet, Energy and emissions saving potential of additive manufacturing: the case of lightweight aircraft components, J. Clean. Prod. 135 (2016) 1559–1570.
[4] T. Al-Samman, G. Gottstein, Room temperature formability of a magnesium AZ31 alloy: examining the role of texture on the deformation mechanisms, Mater. Sci. Eng. A 488 (2008) 406–414.
[5] R. Von Mises, Mechanik der plastischen Formänderung von Kristallen, Z. Angew. Math. Mech. 8 (1928) 161–185.
[6] S.G. Hong, S.H. Park, C.S. Lee, Role of {10–12} twinning characteristics in the deformation behavior of a polycrystalline magnesium alloy, Acta Mater. 58 (2010) 5873–5885.
[7] P.G. Partridge, E. Roberts, The formation and behaviour of incoherent twin boundaries in hexagonal metals, Acta Metall. 12 (1964) 1205–1210.
[8] X.L. Nan, H.Y. Wang, L. Zhang, J.B. Li, Q.C. Jiang, Calculation of Schmid factors in magnesium: analysis of deformation behaviors, Scripta Mater. 67 (2012) 443–446.
[9] C.S. Robert, Magnesium and Its Alloys, John Wiley, New York, 1960.

[10] L. Wu, S.R. Agnew, D.W. Brown, G.M. Stoica, B. Clausen, A. Jain, D.E. Fielden, P. K. Liaw, Internal stress relaxation and load redistribution during the twinning–detwinning-dominated cyclic deformation of a wrought magnesium alloy, ZK60A, Acta Mater. 56 (2008) 3699–3707.
[11] B. Clausen, C.N. Tomé, D.W. Brown, S.R. Agnew, Reorientation and stress relaxation due to twinning: modeling and experimental characterization for Mg, Acta Mater. 56 (2008) 2456–2468.
[12] M.R. Barnett, M.D. Nave, A. Ghaderi, Yield point elongation due to twinning in a magnesium alloy, Acta Mater. 60 (2012) 1433–1443.
[13] K. Anten, B. Scholtes, Formation of macroscopic twin bands and inhomogeneous deformation during cyclic tension-compression loading of the Mg-wrought alloy AZ31, Mater. Sci. Eng. A 746 (2019) 217–228.
[14] S. Hwang, M.H. Park, Y. Bai, A. Shibata, W. Mao, H. Adachi, M. Sato, N. Tsuji, Mesoscopic nature of serration behavior in high-Mn austenitic steel, Acta Mater. 205 (2021) 116543.
[15] M.C. Jo, J.H. Choi, H. Le, A. Zargaran, J.H. Ryu, S.S. Sohn, N.J. Kim, S. Lee, Effects of solute segregation on tensile properties and serration behavior in ultra-high-strength high-Mn TRIP steels, Mater. Sci. Eng. A 740–741 (2019) 16–27.
[16] H. Liu, S. Liu, C. Wei, L. Qian, Y. Feng, F. Zhang, Effect of grain size on dynamic strain aging behavior of C-bearing high Mn twinning-induced plasticity steel, J. Mater. Res. Technol. 15 (2021) 6387–6394.
[17] H. Halim, D.S. Wilkinson, M. Niewczas, The Portevin–Le Chatelier (PLC) effect and shear band formation in an AA5754 alloy, Acta Mater. 55 (2007) 4151–4160.
[18] Y. Cai, S. Yang, S. Fu, D. Zhang, Q. Zhang, Investigation of portevin–Le Chatelier band strain and elastic shrinkage in al-based alloys associated with Mg contents, J. Mater. Sci. Technol. 33 (2017) 580–586.
[19] B.S. Shariat, Y. Li, H. Yang, Y. Wang, Y. Liu, On the Lüders band formation and propagation in NiTi shape memory alloys, J. Mater. Sci. Technol. 116 (2022) 22–29.
[20] D. Saletti, S. Pattofatto, H. Zhao, Measurement of phase transformation properties under moderate impact tensile loading in a NiTi alloy, Mech. Mater. 65 (2013) 1–11.
[21] H. Yu, Y. Xin, H. Zhou, R. Hong, L. Zhao, Q. Liu, Detwinning behavior of Mg–3Al–1Zn alloy at elevated temperatures, Mater. Sci. Eng. A 617 (2014) 24–30.
[22] S.G. Hong, S.H. Park, C.S. Lee, Enhancing the fatigue property of rolled AZ31 magnesium alloy by controlling {10-12} twinning-detwinning characteristics, J. Mater. Res. 25 (2010) 784–792.
[23] D. Caillard, Dynamic strain ageing in iron alloys: the shielding effect of carbon, Acta Mater. 112 (2016) 273–284.
[24] A. van den Beukel, Theory of the effect of dynamic strain aging on mechanical properties, Phys. Status Solidi 30 (1975) 197–206.
[25] S.J. Lee, J. Kim, S.N. Kane, B.C. De Cooman, On the origin of dynamic strain aging in twinning-induced plasticity steels, Acta Mater. 59 (2011) 6809–6819.
[26] L. Chen, H.S. Kim, S.K. Kim, B.C. De Cooman, Localized deformation due to Portevin–LeChatelier effect in 18Mn–0.6C TWIP austenitic steel, ISIJ Int. 47 (2007) 1804–1812.